ORIGINAL RESEARCH PAPER

Structural Features of $La_{0.55}Ca_{0.45}A_{0.50}Co_{0.50}O_3$ (A=Mg, Mn) Nanoparticles Over Photo-Degradation of Methyl Blue

Hamid Yousefi [1], Ahmad Gholizadeh [1]*, Zahra Mirbeig Sabzevari [2], Azim Malekzadeh [2]

[1] *School of Physics, Damghan University (DU), Damghan, Islamic Republic of Iran*
[2] *School of Chemistry, Damghan University (DU), Damghan. Iran*

Received: 2017-08-07 Accepted: 2017-10-04 Published: 2017-12-20

ABSTRACT

In this paper, $La_{0.55}Ca_{0.45}A_{0.5}Co_{0.5}O_3$(A=Mg, Mn) nanoparticles were synthesized by citrate method. The samples were characterized using the techniques of using X-ray diffraction (XRD), transmission electron microscopy (TEM), Fourier transform infrared (FTIR) and UV-Vis spectroscopy. The structure was analyzed by Rietveld fitting of the XRD pattern by using X'Pert package and Fullprof program, these shows that the samples have perovskite structure. The calculated values of crystallite size, particle size and band gap energy of $La_{0.55}Ca_{0.45}Mg_{0.5}Co_{0.5}O_3$ are much less than $La_{0.55}Ca_{0.45}Mg_{0.5}Co_{0.5}O_3$. The effects of three operational parameters including irradiation time, pH, and the catalyst amount on the photocatalytic activity of the product on the degradation of methyl blue (MB) under solar condition were studied. The photocatalytic degradation efficiency of MB solution over $La_{0.55}Ca_{0.45}Mn_{0.5}Co_{0.5}O_3$ nanoparticles is higher than that over $La_{0.55}Ca_{0.45}Mg_{0.5}Co_{0.5}O_3$ nanoparticles. 96 % degradation is obtained in an aqueous solution at pH=2.33 and containing 30 mg $La_{0.55}Ca_{0.45}Mg_{0.5}Co_{0.5}O_3$ catalyst after 30 minutes.

Keywords: *Nanoparticles; Cobaltite Perovskite; Structural Properties; UV-Visible; Photo-Degradation.*

How to cite this article

Yousefi H, Gholizadeh A, Mirbeig Sabzevari Z, Malekzadeh A. Structural Features of $La_{0.55}Ca_{0.45}A_{0.50}Co_{0.50}O_3$ (A=Mg, Mn) Nanoparticles Over Photo-Degradation of Methyl Blue. J. Nanoanalysis., 2017; 4(4): 324-333. DOI: 10.22034/jna.2017.542780.1024

INTRODUCTION

Industries such as textile, leather, paper, plastics, etc., use dyes in order to color their products and also consume substantial volumes of water. As a result, they generate a considerable amount of colored wastewater. Specified amounts of them are lost in the process of their manufacturing and utilization and often cause environmental pollution problems. Nowadays, regulation on the discharge of dye-polluted colored wastewater has been getting stringent in many countries [1-4]. The presence of even small amounts of dyes in water, less than 1 ppm for some dyes, is highly visible and undesirable. It is estimated that more than 100,000 commercially available dyes with over 7×10^5 tons of dyestuff are produced annually [5-8].

The removal of color from textile dye baths is one of the most difficult problems in the field of environmental chemistry. Different techniques were applied such as adsorption, oxidation, reduction, electrochemical, and membrane filtration [9]. Several methods like physical, chemical and biological methods have been

* Corresponding Author Email: gholizadeh@du.ac.ir

investigated for the removal of dye materials from contaminated water. Among the proposed methods, removal of dyes by adsorption technology has been regarded as a competitive method for high efficiency, economic feasibility, and simplicity of design/operation. Moreover, adsorption of dyes on inorganic supports like silica is important to produce pigments [10-12].

Nevertheless, there is a general agreement that atrazine degradation products are substantially less toxic than the parent compound [13]. The mobility of the photogenerated carriers (including holes and electrons) significantly influences the photocatalytic efficiency and the higher photogenerated carrier mobility enhances the photocatalytic performance. Additionally, the valence band position of a semiconductor is important to the photocatalytic activity of the semiconductor. Oxidative activity and the photocatalytic property of the material are higher when the valence band of a semiconductor is deeper [14]. These materials, for their activation, demand higher photon energy, which could be near-UV or in UV range [15-18]. However, since UV occupies just 4% of whole solar energy, the technology becomes difficult to widen the application. Therefore, it is indispensable and urgent to develop a sunlight sensitive photocatalyst for wastewater treatment. To develop a sunlight sensitive photocatalyst either need an appropriately band-gap engineered material or the material to possess satisfactory characteristics which are brought out by its defect nature [14].

In this work, we prepared $La_{0.55}Ca_{0.45}$(Mg or Mn)$_{0.5}Co_{0.5}O_3$ by citrate precursor method. First, geometric parameters of the samples including crystallite size and particle size are studied using X-ray diffraction (XRD) measurement and transmission electron microscopy (TEM). Then, the attempt was made to explain their structural properties and the influence of substituting Mg and Mn on the photocatalytic activity of $La_{0.55}Ca_{0.45}$(Mg or Mn)$_{0.5}Co_{0.5}O_3$ in the removal of dyes by chemical oxidation method. The chemical structure of Methyl Blue (MB, $C_{37}H_{27}N_3Na_2S_3O_9$, triphenyl methane) as a kind of dye that has been used widely is shown in Fig. 1 [19]. The samples have been used as the photo-catalyst under ambient sunlight for decolonization of Methyl blue.

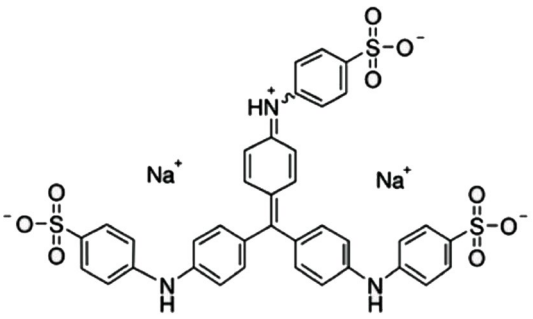

Fig. 1. Chemical structure of methyl blue dye.

EXPERIMENTAL SECTION

The samples of $La_{0.55}Ca_{0.45}A_{0.5}Co_{0.5}O_3$ (A=Mg, Mn) were prepared according to the literature by the citrate method using metal nitrate precursor in the presence of citric acid [20-21]. Solutions of appropriate mole numbers of metal nitrates and citric acid (equal to the total number of nitrate ions moles) in 15 mL distilled water were evaporated at 80°C and 150°C overnight. The samples were completely powdered after each drying. Resulting materials were powdered and calcined at 900°C for 5 h.

The XRD pattern has been recorded using a Bruker AXS diffractometer D8 ADVANCE (Bruker-AXS, Karlsruhe, Germany) with CuKα radiation in the range of 2θ=10-80° at room temperature (RT). The crystallite size of the samples is calculated by using Scherrer's equation as follows [22]:

$$D = \frac{0.94\,\lambda}{\beta_{hkl}\cos\theta} \quad (1)$$

Here, β_{hkl} is the full-width at half-maximum of the diffraction peak at around 47°. In this method, the increase of peak broadening is due to decrease of crystallite size. The particle size of C60M50 sample was investigated by the TEM (LEO Model 912AB, GmbH, Oberkochen, Germany) analysis. Size distribution histogram is fitted by using a log-normal function as follow [23]:

$$P(d) = \frac{1}{D\sigma_d\sqrt{2\pi}}\exp\left\{-\frac{1}{2\sigma_d^2}\ln^2\left(\frac{D}{D_{TEM}}\right)\right\} \quad (2)$$

Where σ_d is the standard deviation of the diameter and D_{TEM} is the mean diameter obtained from the TEM results.

The FT-IR spectra of samples were recorded with a PERKIN-ELMER FT-IR spectrometer (Perkin-Elmer Spectrum RXI FT-IR System) in the wave number range of 300-4000 cm^{-1}. Optical absorption spectra of the samples have been recorded between 200 and 1000 nm wavelengths with a HP-UV-Vis system (Analytic Jena AG, Jena, Germany) to study optical and photocatalytic characteristics of the samples. Band gap energies of the samples have been calculated using optical absorption spectra recorded between 200 and 1100 nm wavelengths same as the literature [24]. The following relation holds between the optical absorption coefficient, α (λ), and the optical band gap energy of a direct band transition, $(\alpha hv)^2=B(hv-E_g)$. Here, B is an energy-independent constant and $\alpha(\lambda)=2.303\ (A(\lambda))/t$ is optical absorption coefficient calculated from the absorption spectra (A(λ)) and also the mean particle size of the sample (t). Band gap energy of the samples is estimated by extrapolating the linear part of $(\alpha hv)^2$ vs. plot. Then, the photocatalytic activity of nanoparticles for degradation of methyl blue aqueous solution is investigated using absorption spectra at wavelengths range of 300-700 nm. Before lighting, the suspension is sufficiently stirred for 30 min to reach adsorption-desorption equilibrium between the catalysts and methyl blue, so that the adsorption in the dark can be discounted. The effect of the absorbent value, contact time, and pH are studied to obtain optimal conditions.

RESULTS AND DISCUSSIONS

Structural Characterization

X-ray diffraction patterns of $La_{0.55}Ca_{0.45}A_{0.5}Co_{0.5}O_3$ (A=Mg, Mn) are shown in Fig. 2. XRD data were analyzed using both the commercial X'Pert High Score package and Fullprof program. Identification of structure type using X'pert package confirms the existence of the main phase with perovskite structure without the presence of impurity phases in the samples. Rietveld analysis of the samples by using Fullprof program indicates all the diffraction peaks of $La_{0.55}Ca_{0.45}Mn_{0.5}Co_{0.5}O_3$ be quite well indexed in rhombohedra structure with the space group R-3c. However, it shows the presence of two-phase orthorhombic system including Pnma II and final Pnma I phases for $La_{0.55}Ca_{0.45}Mg_{0.5}Co_{0.5}O_3$. The best fit with the least difference is carried out as shown in Fig. 2. The crystallite size and the lattice parameters of the samples are given in Table 1. The crystallite size of $La_{0.55}Ca_{0.45}Mn_{0.5}Co_{0.5}O_3$ is much less than $La_{0.55}Ca_{0.45}Mg_{0.5}Co_{0.5}O_3$.

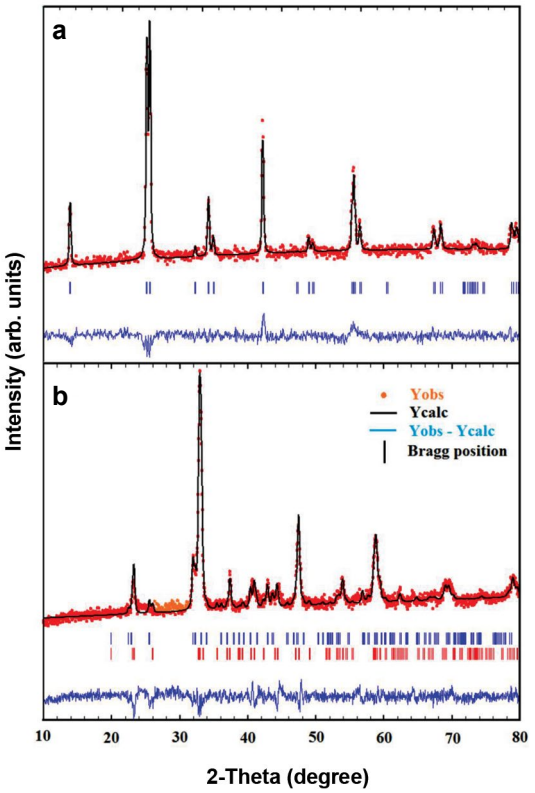

Fig. 2. Rietveld analysis of $La_{0.55}Ca_{0.45}A_{0.5}Co_{0.5}O_3$ using Fullprof program. The circle sings represent the raw data. The solid line represents the calculated profile. Vertical bars in (Mn) indicate the position of Bragg peaks for rhombohedral with space group R-3c and in (Mg) the position of Bragg peaks for orthorhombic structure with space groups Pnma II and Pnma I, respectively. The lowest curve is the difference between the observed and the calculated patterns.

TEM micrograph and particle size distribution of $La_{0.55}Ca_{0.45}A_{0.5}Co_{0.5}O_3$ (A=Mg, Mn) are shown in Fig 3. Fitting of the size distribution histogram by using a log-normal function indicates that the mean diameter calculated for $La_{0.55}Ca_{0.45}Mn_{0.5}Co_{0.5}O_3$ and $La_{0.55}Ca_{0.45}Mg_{0.5}Co_{0.5}O_3$ nanoparticles are 46 nm and 84 nm, respectively. The result is different from the crystallite size calculated by XRD measurement. The difference is related to the irregular shape of nanoparticles with spherical, spheroidal and polygon morphologies which are observed in the TEM micrographs.

Table 1: Crystallite size, structure type and unit cell parameters of the samples. A is the Pnma I or Pnma II Share (%)

Sample	Abbreviation sample #	Structure	Space group	A (%)	lattice Parameters	D (nm)
$La_{0.55}Ca_{0.45}Mn_{0.5}Co_{0.5}O_3$	*Mn*	*Rhombohedral*	*R-3c*	-----	*a=b=c=5.388 (Å), α=β =γ= 60.371 (°)*	*24*
$La_{0.55}Ca_{0.45}Mg_{0.5}Co_{0.5}O_3$	*Mg*	*Orthorhombic*	*Pnma I*	*90*	*a=5.3004(Å) , b=7.7650 (Å), c=5.5582(Å)*	*32*
			Pnma II	*10*	*a=5.4081(Å), b=7.6219(Å), c=5.2994(Å)*	

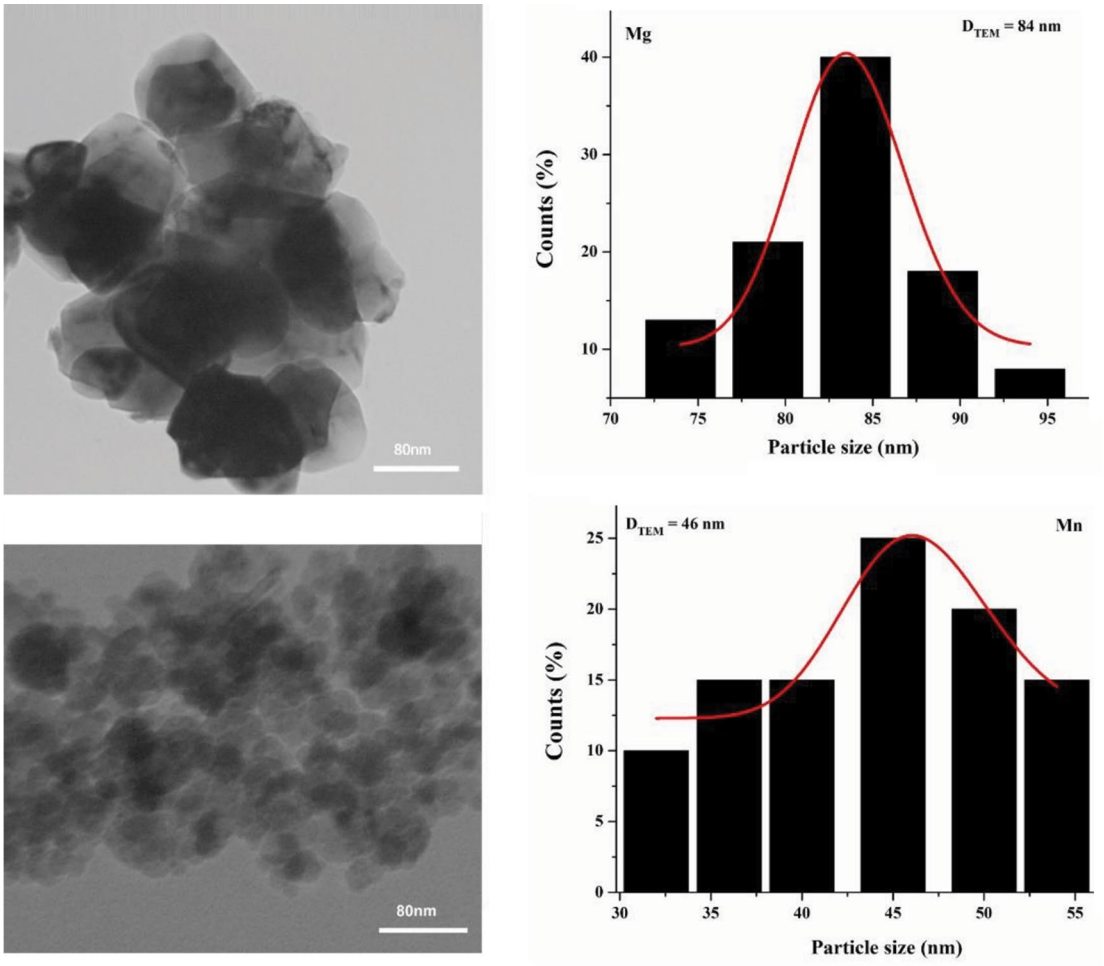

Fig. 3. TEM micrographs and size distribution histograms of $La_{0.55}Ca_{0.45}A_{0.5}Co_{0.5}O_3$.

Optical Characterization

Variation of $(\alpha h\upsilon)^2$ with photon energy hυ for the nanoparticles is shown in Fig. 4. One can observe that the plots are linear over a wide range of photon energy suggesting direct transitions. The direct band gap energies of the nanoparticles 1.91 eV and 2.85 eV were calculated using Tauc equation, from the intersections of the straight line with the energy axis [24]. The values of the band gap energy show metallic behavior for $La_{0.55}Ca_{0.45}Mn_{0.5}Co_{0.5}O_3$, but, semiconductor for $La_{0.55}Ca_{0.45}Mg_{0.5}Co_{0.5}O_3$.

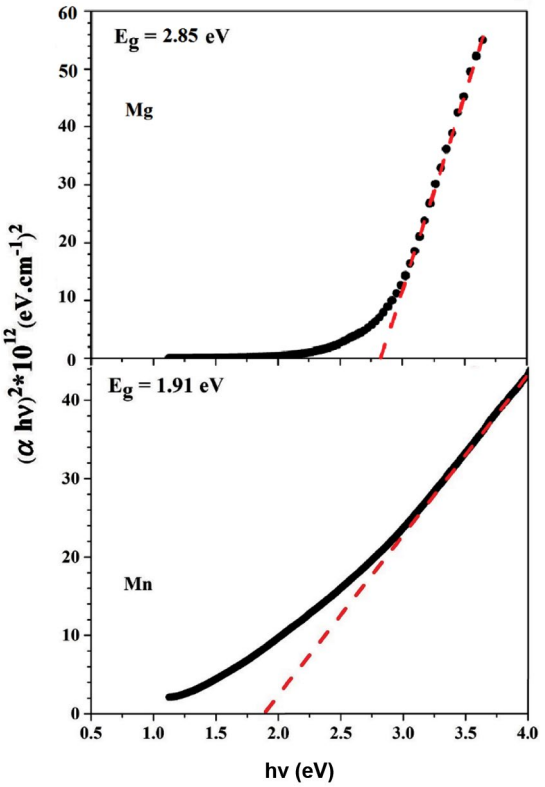

4. The plot of the Tauc's equation to obtain band gap of $La_{0.55}Ca_{0.45}A_{0.5}Co_{0.5}O_3$ nanoparticles.

Photocata1tic degradation of MB

For all the experiments mentioned here, the MB dye concentration was kept constant to 25mg per 1 liter of water. This was used as stalk solution, out of which 20 ml solution was used for all individual experiments. In this aliquot, 10 mg (500 mg/l) of catalyst was added, and the solution was subjected to ambient sunlight.

The absorption spectra of the samples were recorded by measuring the absorbance at 607 nm corresponding to the maximum absorption wavelength of MB with UV–visible absorption spectroscopy. The photocatalytic degradation rate (DC) was calculated by the following formula [25-26]:

$$P(d) = \frac{1}{D\sigma_d\sqrt{2\pi}} \exp\left\{-\frac{1}{2\sigma_d^2}\ln^2\left(\frac{D}{D_{TEM}}\right)\right\} \quad (3)$$

Where A_o is the initial absorbance of MB solution without any exposure, A_t is the absorbance of MB after photo-irradiation for time (t).

The photocatalytic reaction rate depends on the concentration of the organic pollutants and can be described by the following kinetic model [27]:

$$Rate = -\left(\frac{dC}{dt}\right) = \left(\frac{kKC}{1+KC}\right) \quad (4)$$

Where C is the concentration of MB (mg/L) at any time, t is the irradiation time, k is the first-order rate constant of the reaction and K is the adsorption constant of the pollutant on the photocatalyst. This equation can be simplified to a pseudo-first-order equation [28]:

$$ln\left(\frac{C}{C_0}\right) = -kKt = K_{obs}t \quad (5)$$

In which cowboys are the observed first-order rate constant of the photo-degradation reaction.

The observed first-order rate constant for the photocatalytic degradation of MB on the nanoparticles was calculated using plots of LnC/C_0 versus irradiation time.

Fig.5 shows the degradation efficiency of MB solutions in the presence 10 mg of $La_{0.55}Ca_{0.45}A_{0.5}Co_{0.5}O_3$ (A=Mn, Mg) nanoparticles under visible light. From this figure, it could be seen that the degradation efficiency of MB with the photo-catalysts in acidic solution is more efficient than more natural than the basic solution. Also, the degradation efficiency of MB solutions in the presence of $La_{0.55}Ca_{0.45}Mn_{0.5}Co_{0.5}O_3$ nanoparticles is higher than $La_{0.55}Ca_{0.45}Mg_{0.5}Co_{0.5}O_3$ nanoparticles.

The reactivity of nanosized materials is often altered or enhanced concerning their bulk counterparts due to size-dependent changes in their redox potentials and high density of the active surface states associated with a large surface-to-volume ratio. Moreover, recombination of electron-hole pairs within the semiconductor particle is drastically reduced as particle size decreases [29]. So, the better photocatalytic activity of $La_{0.55}Ca_{0.45}Mn_{0.5}Co_{0.5}O_3$ than $La_{0.55}Ca_{0.45}Mg_{0.5}Co_{0.5}O_3$ can be related to smaller particle size calculated by using XRD measurement and TEM and also observed metallic behavior in this sample with respect to another. So we use $La_{0.55}Ca_{0.45}Mn_{0.5}Co_{0.5}O_3$ nanopartricles and study to detect optimum term for this aqueous. In below, photocatalytic activity

of this sample is subjected further.

We use different values of HCl (0.1N) (Fig. 6) in the solution to discover that in which pH of the aqueous with $La_{0.55}Ca_{0.45}Mn_{0.5}Co_{0.5}O_3$ catalyst has a maximum degradation efficiency. After examining the 0.01, 0.05, 0.1 cc of the acid, we found that the solution with 0.1 cc HCl (pH=2.33) and $La_{0.55}Ca_{0.45}Mn_{0.5}Co_{0.5}O_3$ nanocatalyst has maximum degradation efficiency between acidic solutions. Fig. 7 shows that the adsorption capacity decreases below pH=3. These variations in adsorption capacities of different catalysts highly dependent on the zero point charges. Because of the amphoteric behavior of most of the semiconductor oxides, an important parameter in the reaction on the semiconductor particle surface is the pH of dispersions, since it influences the surface charge properties of photo-catalyst, the anionic dye molecule is negatively charged, and so low pH favors adsorption on the catalyst surface [30].

Fourier transform infrared (FT-IR) spectroscopy results of fresh $La_{0.55}Ca_{0.45}A_{0.50}Co_{0.50}O_3$ (A=Mn, Mg) and used one after photocatalytic tests at pH=2.33 are shown in Fig. 8. Similar FT-IR spectrum is observed for fresh and spent samples. The broad absorption band at 615 cm^{-1} is related to the asymmetry lengthening of the Mn-O vibrations of MnO_6 octahedral in perovskite structure [31]. A sharper band was related to a more symmetrical structure. The widening of this band and/or the appearance of a shoulder was reported to be an indication of a structure with lower symmetry. A shoulder in the perovskites at 540 cm^{-1} is cited to be a characteristic of a rhombohedral structure [32]. Results of Fig. 8 can be accounted for a more symmetric rhombohedra perovskite structure after degradation. No MB residual, however, is observed after photocatalytic degradation over $La_{0.55}Ca_{0.45}A_{0.50}Co_{0.50}O_3$ nanoparticles. It can be concluded that adsorption of MB over the surface of the catalysts is followed by degradation. The peaks at 1636 and 3422 cm^{-1} in fresh sample are assigned to the O-H vibrations of trace of water on the sample. The $La_{0.55}Ca_{0.45}A_{0.50}Co_{0.50}O_3$ is found to be an efficient photocatalyst under solar irradiation.

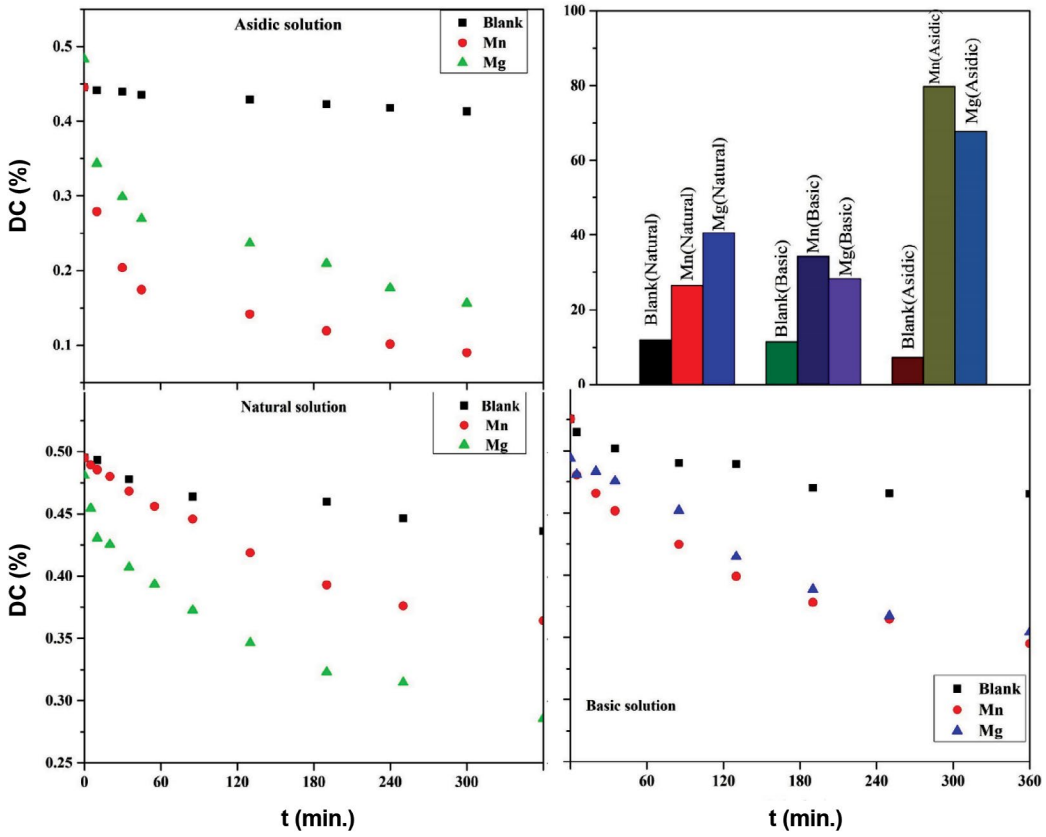

Fig. 5. Degradation efficiency of MB with the photocatalyst in natural, basic (in 360 min) and acidic solutions (in 300 min).

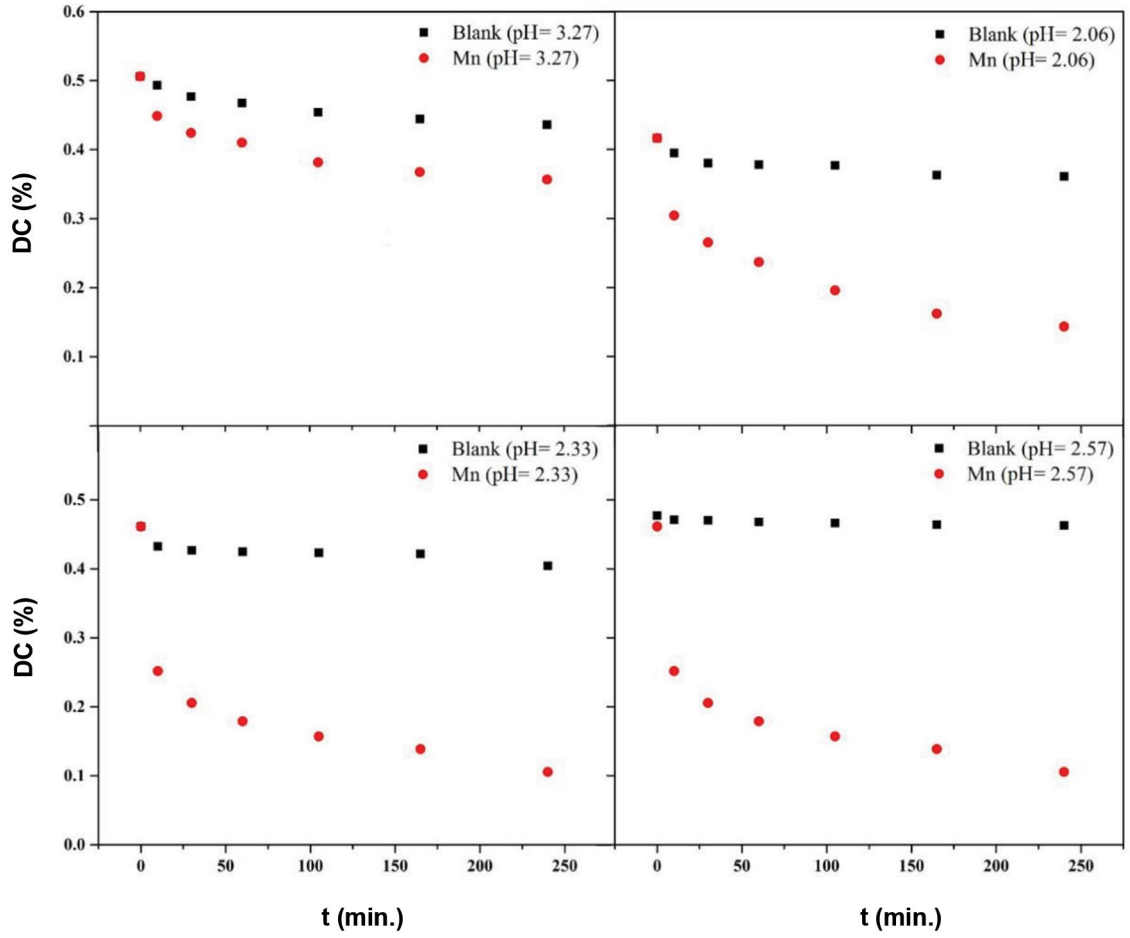

Fig. 6. Degradation efficiency of MB with the photocatalysts in acidic solutions.

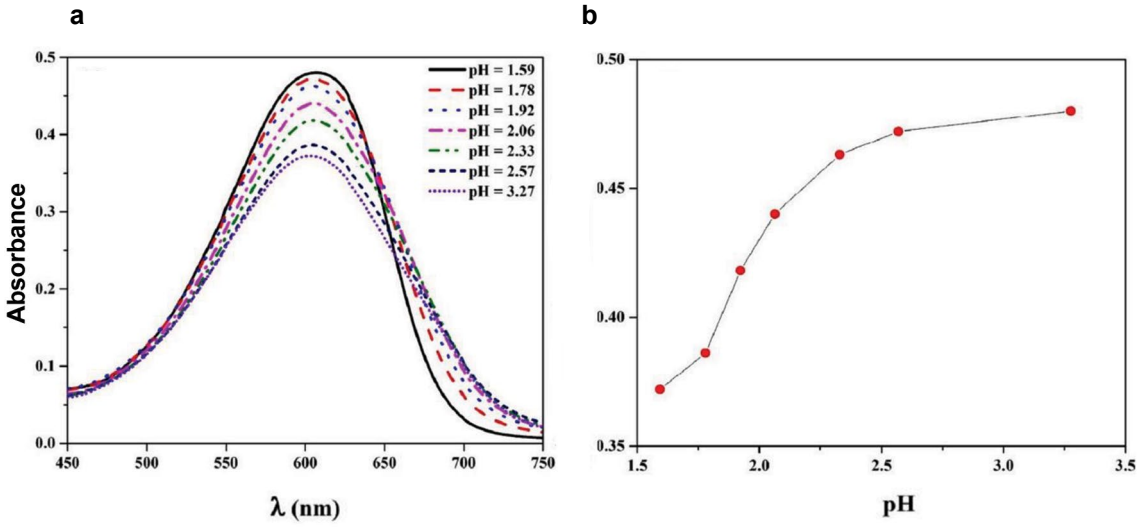

Fig. 7. Effect of pH on the adsorption capacity of methyl blue on $La_{0.55}Ca_{0.45}Mn_{0.5}Co_{0.5}O_3$ catalyst (b) Absorption spectrum of a 25 ppm MB solution in different pH.

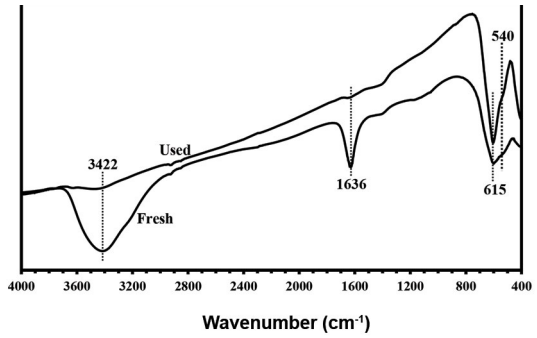

Fig. 8. FT-IR spectrum of fresh and used $La_{0.55}Ca_{0.45}Mn_{0.5}Co_{0.5}O_3$ photocatalyst.

The degradation of MB on $La_{0.55}Ca_{0.45}Mn_{0.5}Co_{0.5}O_3$ was done by varying catalyst amounts from 5 to 50 mg for the dye solution at maximized pH of 2.33 (Fig. 9). Maximum degradation is observed with 30 mg of the catalyst. This could be due to the fact that by increasing the mass of catalyst, higher surface area and active sites of the catalyst is available. Also, the excess amount of $La_{0.55}Ca_{0.45}Mn_{0.5}Co_{0.5}O_3$ above this dosage did not significantly enhance the degradation as shown in Fig.9. This is due to aggregation of catalyst particles, which reduced the surface area between the reaction solution and the photocatalyst. The increase in opacity and light scattering by the particles may be other reasons for the degradation rate [33-34]. This phenomenon can be ascribed to the reason that the number of the reactive sites can be increased when the amount of the catalysts was increasing. However, these nanoparticles may have a tendency to aggregate when their quantity is in excess, thus contributing to the decrease of the reactive sites. Besides, excess amount of the catalyst may exist as the scavenger of hydroxyl radicals [35-37]. Therefore, we choose 30 mg catalyst as the optimum amount of $La_{0.55}Ca_{0.45}Mn_{0.5}Co_{0.5}O_3$ in aqueous solution and investigate the degradation of MB in this solution (Fig. 9).

Photo-Fenton degradation of MB in aqueous solution in the presence of $La_{0.55}Ca_{0.45}Mn_{0.5}Co_{0.5}O_3$ photocatalysts at room temperature under pH=2.33 are shown in Fig. 10. In general, the kinetics of photocatalytic degradation of organic pollutants on the semiconducting oxide has been established and can be described well by the apparent first-order reaction in $(C_0/C_t) = k_{app}\, t$, where k_{app} is the apparent rate constant, c_0 is the concentration of MB after darkness adsorption for 30 min and c_t is the concentration of MB at time t. The inset of Fig. 11 shows the linear relation of $ln\,(C_0/C_t)$ versus irradiation time for degradation of MB [38]. Also, the photocatalytic degradation of MB over $La_{0.55}Ca_{0.45}Mn_{0.5}Co_{0.5}O_3$ catalyst, obeys the pseudo-zero-order regarding modified Langmuir-Hinshelwood (LW-H) model [39].

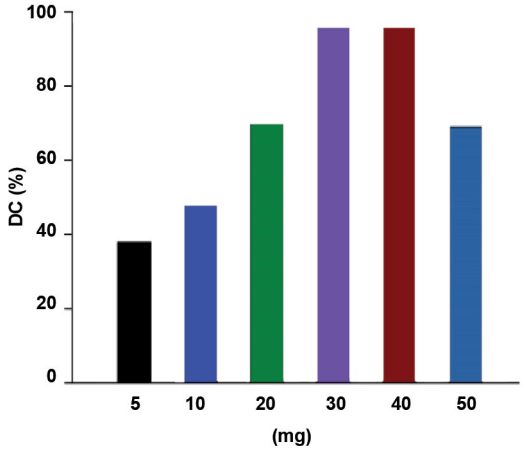

Fig. 9. Effect of the amount of catalyst on the degradation of MB (C_0=25 ppm, pH=2.33, time of irradiation=30 min, temperature=28–32 °C).

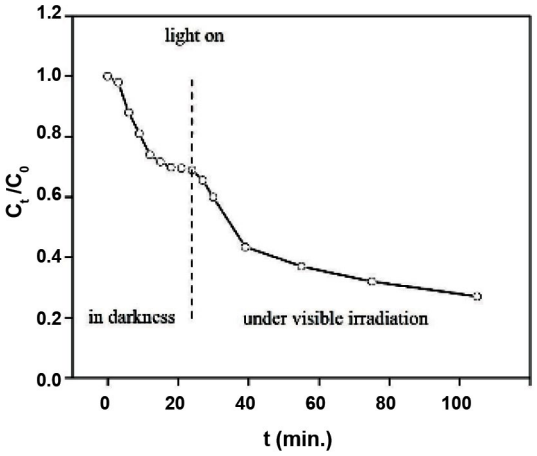

Fig. 10. Photo-Fenton degradation of MB in the presence of the catalyst at room temperature under pH=2.33.

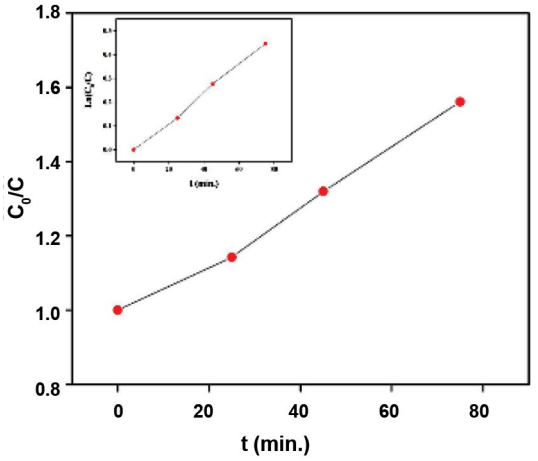

Fig. 11. Photodegradation of methyl blue (MB) under solar irradiation in the presence of $La_{0.55}Ca_{0.45}Mn_{0.5}Co_{0.5}O_3$ sample (inset shows its vs. time graph).

CONCLUSIONS

$La_{0.55}Ca_{0.45}A_{0.5}Co_{0.5}O_3$(A=Mg, Mn) nanoparticles prepared by citrate method were characterized using X-ray diffraction measurement, transmission electron microscopy, Fourier transform infrared and UV-Vis spectroscopy. The structural characterization of the samples using X'Pert package and Fullprof program is evidence for the presence of the rhombohedral structure (space group R-3c) in $La_{0.55}Ca_{0.45}Mn_{0.5}Co_{0.5}O_3$ and orthorhombic structure (two-phase system Pnma I and Pnma II) in $La_{0.55}Ca_{0.45}Mg_{0.5}Co_{0.5}O_3$. The calculated value of crystallite size and particle size of $La_{0.55}Ca_{0.45}Mn_{0.5}Co_{0.5}O_3$ is much less than $La_{0.55}Ca_{0.45}Mg_{0.5}Co_{0.5}O_3$. $La_{0.55}Ca_{0.45}A_{0.5}Co_{0.5}O_3$ (A=Mg, Mn). Nanoparticles prepared by the citrate-nitrate method were characterized by FT-IR and UV-Vis spectroscopy. The values of the band gap energy calculated using Tauc equation are 1.31 eV and 3.58 eV that show metallic behaviour for $La_{0.55}Ca_{0.45}Mn_{0.5}Co_{0.5}O_3$, but semiconductor behaviour for $La_{0.55}Ca_{0.45}Mg_{0.5}Co_{0.5}O_3$. There is no difference between the FT-IR of the fresh and used samples with the same concentration. No MB residual is observed after photocatalytic degradation for all solutions that we examined in this work over $La_{0.55}Ca_{0.45}A_{0.5}Co_{0.5}O_3$ (A=Mn, Mg) nanoparticles. Also adsorption of MB over the surface of $La_{0.55}Ca_{0.45}A_{0.5}Co_{0.5}O_3$ (A=Mn, Mg) nanoparticles is followed by the degradation. The photocatalytic activity of the product was studied for degradation of an aqueous solution of methyl blue under solar condition. The results show that three operational parameters including irradiation time, pH, and the catalyst amount strongly affect the dye degradation. The degradation efficiency of MB solutions in the presence of 10 mg $La_{0.55}Ca_{0.45}Mn_{0.5}Co_{0.5}O_3$ nanoparticles under visible light indicate to be higher than $La_{0.55}Ca_{0.45}Mg_{0.5}Co_{0.5}O_3$ nanoparticles. Also, the solution with 0.1 cc HCl (pH=2.33) and 30 mg of $La_{0.55}Ca_{0.45}Mn_{0.5}Co_{0.5}O_3$ nanocatalyst has 96 % degradation efficiency after 30 minutes between asidic solutions.

CONFLICT OF INTEREST

The authors declare that there is no conflict of interests regarding the publication of this manuscript.

REFERENCES

1. K. Tanaka, P. Kanjana and H. Teruaki, *Water Res*., 34, 327 (2000).
2. H. Lachheb, E. Puzenat, A. Houas, M. Ksibi, E. Elaloui, Ch. Guillard, J.-M. Herrmann, *Appl. Catal*., B 39, 75 (2002).
3. G. Crini, *Bioresour. Technol*., 97, 1061 (2006).
4. K. Ravikumar,, B. Deebika, and K. Balu, *J. Hazard. Mater*., 122, 75 (2005).
5. G. McMullan, C. Meehan, A. Conneely, N. Kirby, T. Robinson, P. Nigam, I. Banat, R. Marchant and W. Smyth, *Appl. Microbiol. Biotechnol*., 56, 81 (2001).
6. N. Soltani, E. Saion, M.Z. Hussein, M. Erfani, A. Abedini, G. Bahmanrokh, M. Navasery and P. Vaziri, *Int. J. Mol. Sci*., 13, 12242 (2012).
7. C. I. Pearce, J. R. Lloyd and J. T. Guthrie, *Dyes pig*., 58, 179 (2003).
8. J.-W. Lee, S.-Ph. Choi, R. Thiruvenkatachari, W.-G. Shim, H. Moon, *Dyes pig*., 69, 196 (2006).
9. I.A. Salem and S. E.-M Mohamed, *Chemosphere*., 41, 1173 (2000).
10. E. Haque, W.J. Jong and H. J. Sung, *J. Hazard. Mater*., 185, 507 (2011).
11. T. Jesionowski, *Dyes pig*., 67, 81 (2005).
12. T. Jesionowski, A. Agnieszka and K. Andrzej, *Color. Technol*., 124, 165 (2008).
13. J.-M. Herrmann, *Catal. Today*, 53, 115 (1999).
14. R. Kitture, S. J. Koppikar, R. Kaul-Ghanekar, S.N. Kale, *J. Phys. Chem. Solids*, 72, 60 (2011).
15. M. Keshmiri, M. Madjid and T. Tom, *Appl. Catal., B* 53, 209 (2004).
16. C. Su, B-Y. Hong and C.-M. Tseng, *Catal. Today,* 96, 119 (2004).
17. G. Sivalingam, K. Nagaveni, M.S. Hegdeb, G. Madras, *Appl. Catal*., B 45, 23 (2003).
18. K. Nagaveni, G. Sivalingam, M.S. Hegde, G. Madras, *Appl. Catal., B* 48, 83 (2004).
19. *HYPERLINK"http://www.sigmaaldrich.com"*www.sigmaaldrich.com.
20. A. Gholizadeh, A. Malekzadeh, M. Ghiasi, *Ceram. Int*., 42,

5707 (2016).

21. A. Gholizadeh, A. Malekzadeh, *Int. J. Appl. Ceram*. Tec., 14, 404 (2017).
22. A. Gholizadeh, *J. Am. Ceram*. Soc., 100, 813 (2017).
23. A. Gholizadeh, H. Yousefi, A. Malekzadeh, F. Pourarian, *Ceram. Int*., 42, 12055 (2016).
24. A. Gholizadeh, N. Tajabor, *Mater. Sci. Semicond. Process*., 13, 162 (2010).
25. K. Wang, L. Yu, Sh. Yin, H. Li, H. Li, *Pure Appl. Chem*., 81, 2327 (2009).
26. Y. Abdollahi, A.H. Abdullah, Z. Zainal and N.A. Yusof, *Int. J. Mol. Sci*., 13, 302 (2011).
27. V. Taghvaei, H.-Y. Aziz and B. Mahdi, *Physica E*., 42, 1973 (2010).
28. X. Xu, R. Lu, X. Zhao, S. Xu, X. Lei, F. Zhang, David G. Evans, *Appl. Catal., B* 102, 147 (2011).
29. F. Zhang, S. Weijie and L. Jing, *Appl. Surf. Sci*., 326, 195 (2015).
30. A. F. Alkaim, A. M. Aljeboree, N. A. Alrazaq, S. J. Baqir, F. H. Hussein, A. J. Lilo, *Asian J. Chem*., 26, 8445 (2014).
31. G. Pecchi, C. Claudia and P. Octavio, *Mater. Res. Bull*., 44, 846 (2009).
32. M. Khazaei, A. Malekzadeh, F. Amini, Y. Mortazavi, A. Khodadadi, Cryst. Res. Technol., 45, 1064 (2010).
33. R. Vinu and M. Giridhar, *Environ. Sci. Technol*., 43, 473 (2008).
34. S.G. Schrank, H.J. José, R.F.P.M. Moreira, H.Fr. Schröder, *Chemosphere*., 60, 644 (2005).
35. X. Yang, W. Chen, J. Huang, Y. Zhou, Y. Zhu, C. Li, *Sci. Rep*., 22, 10632 (2015).
36. Y. Kuang, Q. Wang, Z. Chen, M. Megharaj, R. Naidub, *J. Colloid Interface Sci*., 410, 67 (2013).
37. H. Bel Hadjltaief, P. Da Costa, M. Elena Galvez and M.B. Zina, *Ind. Eng. Chem. Res.*, 52, 16656 (2013).
38. F. Wang, Sh. Min, Y. Han, L Feng, *Superlattices Microstruct*., 48,170 (2010).
39. M. Zhou, Y. Jiaguo and Y. Huogen, *J. Mol. Catal. A: Chem*., 313, 107 (2009).